Supplemental Information to 'Fluid viscoelasticity drives self-assembly of particle trains in a straight microfluidic channel'

DIRECT NUMERICAL SIMULATIONS

Direct Numerical Simulations (DNS) have been used to compute the fluid dynamics of a system of three spherical, rigid, non-Brownian particles with diameter d suspended in a viscoelastic fluid flowing in a cylindrical microchannel with diameter D and length L (see Figure 1a). A Cartesian reference frame was chosen with the origin at the center of the inlet section with the z-axis denoting the flow direction. The particles were initially aligned along the channel centerline and, for symmetry, stay there during the whole simulation, and do not rotate but only translate. The wall was denoted by $\partial\Omega_{\rm w}$, the inflow and outflow channel sections by $\partial\Omega_{\rm in}$ and $\partial\Omega_{\rm out}$, respectively, and the boundary of the $i-$th particle by ∂P_i.

The governing equations are the mass and momentum balance equations that, assuming incompressibility and negligible inertia for both fluid and particles, read as:

$$\nabla \cdot \boldsymbol{u} = 0, \tag{1}$$

$$\nabla \cdot \boldsymbol{\sigma} = \boldsymbol{0}, \tag{2}$$

where $\boldsymbol{u}$ is the fluid velocity and $\boldsymbol{\sigma}$ is the total stress tensor, expressed as:

$$\boldsymbol{\sigma} = -p\boldsymbol{I} + 2\eta_{\rm s}\boldsymbol{D} + \sum_{k=1}^{m} \boldsymbol{\tau}_k. \tag{3}$$

In Eq. (3), p, $\boldsymbol{I}$, $\eta_{\rm s}$ and $\boldsymbol{D} = (\nabla\boldsymbol{u} + (\nabla\boldsymbol{u})^T)/2$ are the pressure, the unity tensor, the viscosity of a Newtonian 'solvent' and the rate-of-deformation tensor, respectively. A multi-mode constitutive model was used where m is the number of modes and $\boldsymbol{\tau}_k$ is the $k-$th contribution to the viscoelastic stress tensor that needs to be specified by choosing a constitutive equation. We chose the Giesekus model, which well describes dilute polymer solutions like the one used in the experiments [1]:

$$\lambda_k \overset{\nabla}{\boldsymbol{\tau}}_k + \frac{\alpha_k\lambda_k}{\eta_k}\boldsymbol{\tau}_k \cdot \boldsymbol{\tau}_k + \boldsymbol{\tau}_k = 2\eta_k\boldsymbol{D}, \tag{4}$$

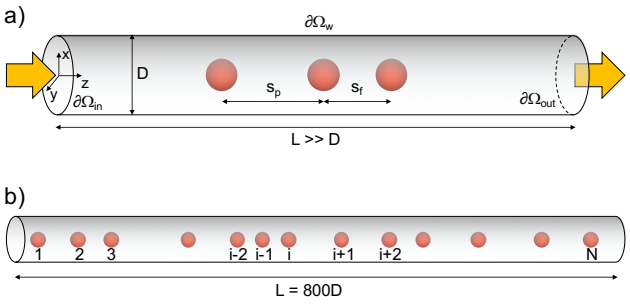

FIG. 1. Schematic representation of the three-particle system (a) and the multi-particle system (b).

where η_k is the $k-$th partial viscosity, λ_k is the $k-$th fluid relaxation time, the symbol $(\overset{\nabla}{})$ denotes the upper-convected time derivative:

$$\overset{\nabla}{\boldsymbol{\tau}}_k \equiv \frac{\partial\boldsymbol{\tau}_k}{\partial t} + \boldsymbol{u}\cdot\nabla\boldsymbol{\tau}_k - (\nabla\boldsymbol{u})^T\cdot\boldsymbol{\tau} - \boldsymbol{\tau}_k\cdot\nabla\boldsymbol{u}, \tag{5}$$

and α_k is the $k-$th anisotropy parameter. The constitutive parameters were evaluated by fitting the rheological data of the HA 1 wt% in PBS. In Table I we report the numerical values of the fitted parameters and in Figure 2 the model predictions (solid lines) compared to the experimental measurements (symbols).

Regarding the boundary conditions, no-slip and rigid-body motion were imposed at the sphere surfaces:

$$\boldsymbol{u} = (0, 0, U_i) \quad \text{on } \partial P_i(t), \tag{6}$$

where i is the particle number and U_i is the particle translational velocity along the flow direction. No-slip conditions were assumed on the channel walls:

$$\boldsymbol{u} = \boldsymbol{0} \quad \text{on } \partial\Omega_{\rm w}. \tag{7}$$

Periodic boundary conditions were prescribed between the inflow and outflow sections, together with a flow rate in inflow:

$$\boldsymbol{u}|_{\partial\Omega_{\rm in}} = \boldsymbol{u}|_{\partial\Omega_{\rm out}}, \tag{8}$$

$$\boldsymbol{t}|_{\partial\Omega_{\rm in}} = -\boldsymbol{t}|_{\partial\Omega_{\rm out}} - \Delta p\boldsymbol{I}, \tag{9}$$

$$\boldsymbol{\tau}_k|_{\partial\Omega_{\rm in}} = \boldsymbol{\tau}_k|_{\partial\Omega_{\rm out}}, \tag{10}$$

$$-\int_{\partial\Omega_{\rm in}} \boldsymbol{u}\cdot\boldsymbol{n}\, dS = Q. \tag{11}$$

In Eq. (9), $\boldsymbol{t} = \boldsymbol{\sigma}\cdot\boldsymbol{n}$ is the traction and $\boldsymbol{n}$ is the outwardly directed unit normal vector. The flow rate Q was imposed through a constraint where the associated Lagrange multiplier is identified as the unknown pressure difference Δp [2].

TABLE I. Values of the parameters of the constitutive equation.

m	2
η_1 [Pa·s]	0.257
η_2 [Pa·s]	0.254
λ_1 [s]	0.0752
λ_2 [s]	0.00848
α_1 [-]	0.283
α_2 [-]	0.49
$\eta_{\rm s}$ [Pa·s]	0.051

As inertia is neglected, no initial condition for the velocity field needs to be specified. On the other hand, since the time-derivative of the viscoelastic stress tensor appears in the constitutive equation, an initial condition for $\boldsymbol{\tau}_k$ is required. We assumed a stress-free initial condition, i.e., that the $k-$the contribution to the stress is zero everywhere in the fluid at the initial time:

$$\boldsymbol{\tau}_k|_{t=0} = \mathbf{0}. \tag{12}$$

To close the set of governing equations, the hydrodynamic force acting on the particles needs to be specified. Under the assumptions of absence of particle inertia, and of no 'external' forces (force-free particle), the $x-$component of the total forces F_i on the spherical surfaces must be zero:

$$F_i = \int_{\partial P_i(t)} (\boldsymbol{\sigma} \cdot \boldsymbol{n})|_z \, dS = 0, \tag{13}$$

where $\boldsymbol{n}$ is the outwardly directed unit normal vector on ∂P_i. Finally, at each time step, the particle positions were updated by integrating the kinematic equations:

$$\frac{dz_i}{dt} = U_i, \tag{14}$$

with initial conditions $z_i|_{t=0} = z_i^0$.

The governing equations were solved by the finite element method with proper stabilization techniques to improve numerical stability [3–7]. A boundary-fitted mesh with triangular elements was used with an adequate number of triangles between the particle surfaces where larger gradients of the flow fields are expected. The Arbitrary Lagrangian-Eulerian (ALE) technique was used to handle the particle motion [8]. Further details on the numerical method used as well as mesh and time convergence tests can be found elsewhere [9].

MULTI-PARTICLE SYSTEM SIMULATIONS

The Direct Numerical Simulations described in the previous section have been carried out on a three-particle system. Several simulations have been performed by varying the two interparticle distances s_p and s_f (see Figure 1a). For each set of distances, we computed the particle velocities U_1, U_2, and U_3 after the initial transient due to the stress development. Hence, the set of two distances (s_p, s_f) and the corresponding three particle velocities form a look-up table that is used to simulate the dynamics of a multi-particle system as described below.

Let us consider a set of N particles already aligned along the channel centerline (see Figure 1b). We assumed that a particle i hydrodynamically interacts only with the trailing particle $i-1$ and the leading particle $i+1$. Hence, the positions of the particles can be computed by integrating the following system of ordinary differential equations:

$$\begin{aligned}
\frac{dz_1}{dt} &= U_1(s_{p,2}, s_{f,2}) \\
\frac{dz_i}{dt} &= U_2(s_{p,i}, s_{f,i}) \quad i = [2, \ldots, N-1] \\
\frac{dz_N}{dt} &= U_3(s_{p,N-1}, s_{f,N1}),
\end{aligned} \tag{15}$$

where z_1, z_2, ..., z_N are the positions of the particles from the inlet to the outlet of the channel. Notice that the leftmost particle of the train (particle 1 in Figure 1b) moves with the velocity of the left particle of the three-particle system. Such velocity depends on the distance $s_{p,2}$ between the particles 1 and 2, and the distance $s_{f,2}$ between the particles 2 and 3 (see Figure 1b). Similarly, the rightmost particle of the train (particle N) has the velocity of the right particle of the three-particle system that depends on $s_{p,N-1}$ and $s_{f,N-1}$. All the other particles move at the velocity of the middle particle of the triplet that depends on the distances with the previous and the next particle. The velocities on the right-hand sides are taken by interpolating the look-up table generated from direct numerical simulations. Initially, three

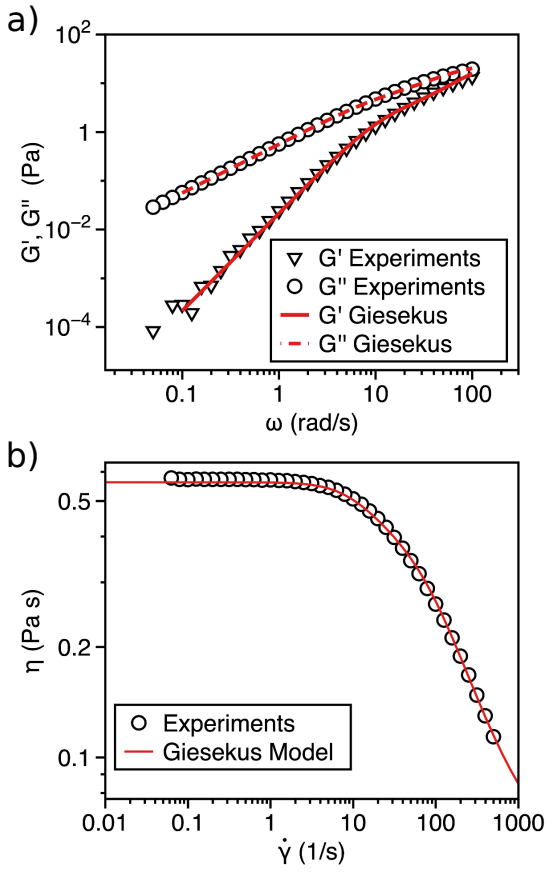

FIG. 2. Predictions (red lines) of the linear viscoelastic moduli (a) and the viscosity (b) obtained by the constitutive model in Eq. 4 with parameters in Table I compared with the rheological measurements (symbols) for the HA 1% in PBS fluid.

particles were positioned near the channel inlet at random distances. When the simulation started, the particles moved along the flow direction and their relative distances change. At random instants, a new particle was positioned on the channel inlet section. The injection interval was taken from a uniform distribution spanning between $[\Delta t_{eq} - \Delta t_r, \Delta t_{eq} + \Delta t_r]$ where Δt_{eq} is related to the particle volume fraction ϕ by $\Delta t_{eq} = V_\mathrm{p}/(\pi R^2 \phi U_\mathrm{max})$ where V_p is the particle volume, $R = D/2$ is the channel radius, and U_max is the fluid velocity at the centerline, which is assumed to be approximately equal to the particle velocity. The parameter Δt_r sets how the initial particle distribution is far from being equally-spaced (equal distances between consecutive particles are obtained for $\Delta t_r = 0$). In this work, we set Δt_r to the maximum possible value before overlapping between the injected particle and the last particle of the train. As soon as a particle crosses the channel outlet, it was removed from the simulation.

The assumption that each particle 'feels' only the adjacent ones might appear quite strong. Such assumption states that the motion of the particle $i+1$ does not directly affect the particle $i-1$ but only the particle i (and $i+2$). The effect on the motion of particle i is then transmitted on the particle $i-1$. In this sense, all the particle motions are coupled only through triplets of particles that directly interact hydrodynamically. To test the validity of this approximation, we perform Direct Numerical Simulations on a system made by six particles suspended in a Newtonian fluid. Figure 3 shows the temporal trends of $s_i^* = (z_i - z_1)/d$, i.e., the difference between the position of a particle i and the position of the first particle of the train normalised by the particle diameter d, obtained from the direct simulations (solid lines) and from the solution of the system of equations in 15. A very good quantitative agreement was found.

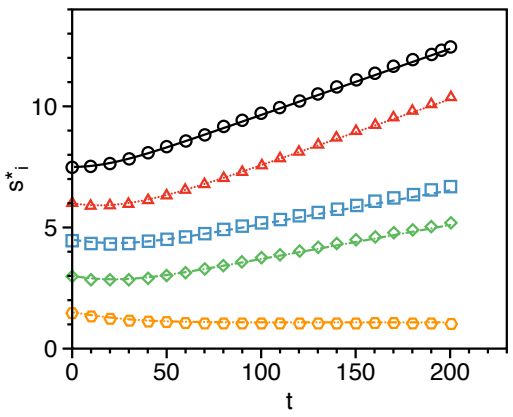

FIG. 3. Comparison between the results obtained from direct numerical simulations (symbols) and the simulations carried out by decomposing the multiparticle system in a set of three-particle systems (lines), as discussed in the text. The investigated problem is a six-particle system in a Newtonian fluid. The data show the temporal trends of the difference between the position of a particle i and the position of the first particle of the train.

DERIVATION OF EQ. 2 OF THE MAIN TEXT

Let us consider a train of spherical particles with diameter d equally distributed on the centerline of a channel with length L and a square cross-section with side H. The distance between the particles is denoted by s. The particle volume fraction is given by:

$$\phi = \frac{N_\mathrm{p} V_\mathrm{p}}{V_\mathrm{c}}, \tag{16}$$

where N_p is the number of particle in the channel, $V_\mathrm{p} = \pi d^3/6$ and $V_\mathrm{c} = H^2 L$ are the particle and channel volume, respectively. Since the particles are equally-spaced, the number of particles becomes $N_\mathrm{p} = L/s$. By substituting these expressions in Eq. 16, we obtain:

$$\phi = \frac{\pi}{6} \frac{N_\mathrm{p} d}{L} \frac{d^2}{H^2}, \tag{17}$$

which can be re-written as:

$$\phi = \frac{\pi}{6} \frac{1}{s^*} \beta^2, \tag{18}$$

where $s^* = L/(N_\mathrm{p} d)$ is the dimensionless interparticle distance and $\beta = d/H$ is the confinement ratio. Notice that the factor $\pi/6$ depends on the channel geometry and corresponds to the maximum packing with spherical particles inscribed in the channel, denoted by ϕ_mp in the main text. Finally, by re-arranging Eq. 18, we obtain the expression of Eq. 2 reported in the main manuscript:

$$s^* \phi = \phi_\mathrm{mp} \beta^2. \tag{19}$$

SI MOVIE

- Video S1: Flow of particles suspended in HA 1 wt% in PBS, at $L_z/H = 800$ (8 cm from the inlet). Volume particle concentration is $\phi = 0.6\%$, and Deborah number $De = 31$. The frame rate is 5000 fps.
- Video S2: Flow of particles suspended in HA 1 wt% in PBS, at $L_z/H = 800$ (8 cm from the inlet). Volume particle concentration is $\phi = 0.6\%$, and Deborah number $De = 62$. The frame rate is 10000 fps.
- Video S3: Flow of particles suspended in HA 1 wt% in PBS, at $L_z/H = 800$ (8 cm from the inlet). Volume particle concentration is $\phi = 1\%$, and Deborah number $De = 31$. The frame rate is 5000 fps.
- Video S4: Flow of particles suspended in HA 1 wt% in PBS, at $L_z/H = 800$ (8 cm from the inlet). Volume particle concentration is $\phi = 1\%$, and Deborah number $De = 62$. The frame rate is 10000 fps.
- Video S5: Flow of particles suspended in HA 0.1 wt% in PBS, at $L_z/H = 800$ (8 cm from the inlet). Volume particle concentration is $\phi = 1.5\%$,

and Deborah number $De = 31$. The frame rate is 5000 fps.

- Video S6: Simulation of flowing particles at $De = 5$, $\phi = 0.4$, and $L_z/H = 0$ (at the inlet).
- Video S7: Simulation of flowing particles at $De = 5$, $\phi = 0.4$, and $L_z/H = 200$ (2 cm from the inlet).
- Video S8: Simulation of flowing particles at $De = 5$, $\phi = 0.4$, and $L_z/H = 400$ (4 cm from the inlet).
- Video S9: Simulation of flowing particles at $De = 5$, $\phi = 0.4$, and $L_z/H = 600$ (6 cm from the inlet).
- Video S10: Simulation of flowing particles at $De = 5$, $\phi = 0.4$, and $L_z/H = 800$ (8 cm from the inlet).

[1] Ronald G Larson, *Constitutive Equations for Polymer Melts and Solutions* (Butterworth-Heinemann, 2013).

[2] Arjen CB Bogaerds, Martien A Hulsen, Gerrit WM Peters, and Frank PT Baaijens, "Stability analysis of injection molding flows," J. Rheology **48**, 765–785 (2004).

[3] Robert Guénette and Michel Fortin, "A new mixed finite element method for computing viscoelastic flows," J. non-Newtonian Fluid Mech. **60**, 27–52 (1995).

[4] Arjen CB Bogaerds, Anne M Grillet, Gerrit WM Peters, and Frank PT Baaijens, "Stability analysis of polymer shear flows using the extended pom–pom constitutive equations," J. non-Newtonian Fluid Mech. **108**, 187–208 (2002).

[5] Alexander N Brooks and Thomas JR Hughes, "Streamline upwind/petrov-galerkin formulations for convection dominated flows with particular emphasis on the incompressible navier-stokes equations," Comput. Methods Appl. Mech. Eng. **32**, 199–259 (1982).

[6] Raanan Fattal and Raz Kupferman, "Constitutive laws for the matrix-logarithm of the conformation tensor," J. non-Newtonian Fluid Mech. **123**, 281–285 (2004).

[7] Martien A Hulsen, Raanan Fattal, and Raz Kupferman, "Flow of viscoelastic fluids past a cylinder at high weissenberg number: stabilized simulations using matrix logarithms," J. non-Newtonian Fluid Mech. **127**, 27–39 (2005).

[8] Howard H Hu, Neelesh A Patankar, and MY Zhu, "Direct numerical simulations of fluid–solid systems using the arbitrary lagrangian–eulerian technique," J. Comput. Phys. **169**, 427–462 (2001).

[9] G. D'Avino, M. A. Hulsen, and P. L. Maffettone, "Dynamics of pairs and triplets of particles in a viscoelastic fluid flowing in a cylindrical channel," Comput. Fluids **86**, 45–55 (2013).